ARTICLES
https://doi.org/10.1038/s41561-018-0069-9
nature geoscience

Export of nutrient rich Northern Component Water preceded early Oligocene Antarctic glaciation

Helen K. Coxall[1]*, Claire E. Huck[2,3], Matthew Huber[4,5], Caroline H. Lear[6], Alba Legarda-Lisarri[7], Matt O'Regan[1], Kasia K. Sliwinska[8,9], Tina van de Flierdt[2], Agatha M. de Boer[1], James C. Zachos[10] and Jan Backman[1]

The onset of the North Atlantic Deep Water formation is thought to have coincided with Antarctic ice-sheet growth about 34 million years ago (Ma). However, this timing is debated, in part due to questions over the geochemical signature of the ancient Northern Component Water (NCW) formed in the deep North Atlantic. Here we present detailed geochemical records from North Atlantic sediment cores located close to sites of deep-water formation. We find that prior to 36 Ma, the north-western Atlantic was stratified, with nutrient-rich, low-salinity bottom waters. This restricted basin transitioned into a conduit for NCW that began flowing southwards approximately one million years before the initial Antarctic glaciation. The probable trigger was tectonic adjustments in subarctic seas that enabled an increased exchange across the Greenland–Scotland Ridge. The increasing surface salinity and density strengthened the production of NCW. The late Eocene deep-water mass differed in its carbon isotopic signature from modern values as a result of the leakage of fossil carbon from the Arctic Ocean. Export of this nutrient-laden water provided a transient pulse of CO_2 to the Earth system, which perhaps caused short-term warming, whereas the long-term effect of enhanced NCW formation was a greater northward heat transport that cooled Antarctica.

The production of deep water in the North Atlantic Ocean plays a vital role in maintaining the global meridional overturning circulation (MOC)[1]. North Atlantic deep water (NADW), the lower branch of the Atlantic part of the MOC (AMOC), forms in the Labrador and Nordic Seas as surface waters cool and densifies. The sinking is largely controlled by an interplay of (1) the stratification at convection sites, determined by the balance of warm salty water from low latitudes, cold freshwater from the Arctic Ocean and local heat and freshwater fluxes, and (2) wind-driven upwelling in the Southern Ocean, which returns deep water to the surface[2,3]. Both factors probably impacted the early Cenozoic MOC state, when Atlantic bathymetry and ocean gateways were different and global temperatures were warmer than today[4,5]. However, to resolve their interplay at the onset of NADW production, referred to here as its palaeo pre-cursor Northern Component Water (NCW), is challenging because the early history of the AMOC remains poorly constrained.

Benthic foraminifera $\delta^{18}O$ and $\delta^{13}C$ records constrain the development of global deep-water circulation by giving insights into subsurface temperatures, salinity and nutrients[5]. A widely held view is that the NCW began filling the Atlantic close to the Eocene–Oligocene greenhouse-to-icehouse climate transition (EOT), ~34 Ma[4,6–9] or earlier[10–13]. Others argue that the emergence of a significant NCW was delayed until the late Miocene[14]. Modelling studies also diverge, with different studies suggesting no NCW[15] during the EOT, a strengthening/onset of bipolar deep-water formation triggered by the Drake Passage deepening[16–18] or an ocean state with a robust NCW throughout[19]. Previous data studies that argue for a late Eocene onset of NCW production assume that the early Cenozoic NCW was nutrient poor with a high ('young') benthic $\delta^{13}C$ signature similar to that of modern well-ventilated NADW[4,10,13,20]. Yet palaeo data needed to characterize the NCW close to source regions is lacking.

To fill this gap, we produced EOT benthic $\delta^{13}C$ and $\delta^{18}O$ records from four deep-sea sites (>1,000 m palaeodepth) in the high latitude North Atlantic (Methods and Supplementary Information). Of these, Site 647 in the Southern Labrador Sea (SLS; 47° N, 34-Myr old palaeolatitude, ~2,000–3,000 m palaeodepth) is the most northerly EOT sequence that contains the calcareous microfossils necessary for $\delta^{18}O$ and $\delta^{13}C$ analysis[21]. Additional data for portions of the late Eocene were generated from Deep Sea Drilling Project (DSDP) Sites 112 and 612, and Inegrated Ocean Drilling Program (IODP) Site U1411 (Fig. 1). The latter two sites should record NCW export in the deep western boundary current (DWBC) (Fig. 1). The data are compared against an Atlantic isotope compilation that incorporates 14 previously investigated sites (Fig. 2). Records of benthic foraminifera Mg/Ca, fish-tooth neodynium (Nd) (reported in epsilon notation, εNd) and planktic foraminifera $\delta^{18}O$ and $\delta^{13}C$ from Sites 647 and U1411 were also generated to provide constraints on the bottom-water temperature (BWT) and provenance, and water

[1]Department of Geological Sciences, Stockholm University, Stockholm, Sweden. [2]Department of Earth Science and Engineering, Imperial College London, London, UK. [3]Ocean and Earth Science, National Oceanography Centre Southampton, University of Southampton, Southampton, UK. [4]Earth, Atmospheric and Planetary Sciences, Purdue University, West Lafayette, IN, USA. [5]Institute for the Study of Earth, Oceans, and Space, University of New Hampshire, Durham, NH, USA. [6]School of Earth and Ocean Sciences, Cardiff University, Cardiff, UK. [7]Department of Earth Sciences, University of Zaragoza, Zaragoza, Spain. [8]Geological Survey of Denmark and Greenland, GEUS, Copenhagen K, Denmark. [9]Department of Marine Organic Biogeochemistry, NIOZ Royal Netherlands Institute for Sea Research, Texel, The Netherlands. [10]Earth & Planetary Sciences Department, University of California, Santa Cruz, USA.
*e-mail: helen.coxall@geo.su.se

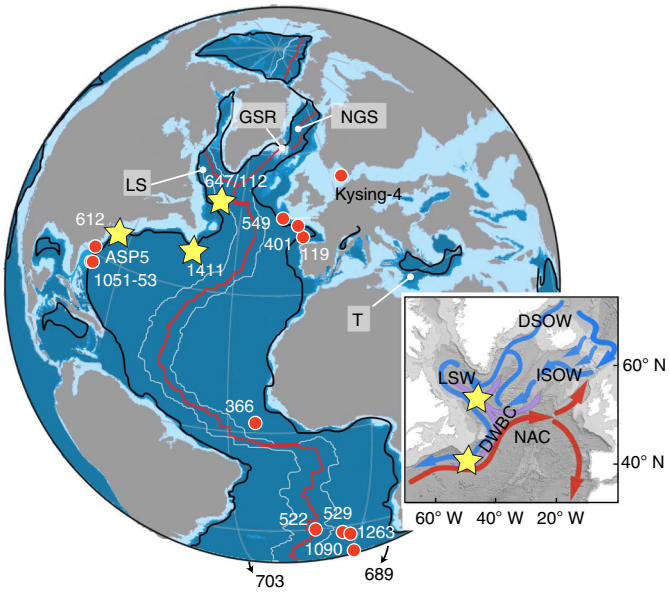

Fig. 1 | Site locations of the sections included in this study. Stars identify the new data sets presented here. Red line, Mid Ocean Ridge 34 Ma; white line, position of the 56=Myr-old isochron; black line, continent–ocean crust boundary. Methods gives details of the palaeogeographic framework and inset map. LS, Labrador Sea, NGS, Norwegian Greenland Sea; T, Tethys Ocean. Inset: path of the major deep (blue) and surface currents today: DSOW, Denmark Strait overflow water; ISOW, Iceland–Scotland overflow water (ISOW); LSW, Labrador Sea water; NAC, North Atlantic current.

column structure (Methods). The results add unique perspectives on the Atlantic end-member deep-water properties and changes in circulation during the EOT.

High nutrient content of late Eocene SLS deep waters

At Site 647 we recognize the typical pattern of $\delta^{18}O$ and $\delta^{13}C$ increase (>1.0‰ Vienna PeeDee Belemnite (VPDB) and ~0.5–1.0‰ VPDB, respectively) between 34 and 33.5 Ma, diagnostic of the early Oligocene Antarctic glaciation, and it includes the peak in $\delta^{18}O$ seen at other sites[22], here referred to as the early Oligocene glacial maximum (EOGM) (Fig. 2). The first novel observation at Site 647 is that before ~35.8 Ma, $\delta^{13}C$ of the SLS bottom water was, on average, 0.5–1‰ VPDB lower than at all the southerly sites. This is opposite to the modern AMOC state, in which northern deep waters have the highest $\delta^{13}C$ due to the sinking of well-ventilated, nutrient-poor surface waters[23]. The low $\delta^{13}C$ value may reflect nutrient accumulation under stratified conditions, analogous to those of the modern North Pacific, that is, the end of the circulation path. This could imply that a southern-sourced deep water filled the SLS during the late Eocene. However, Site 647 fish debris εNd, an isotopic tracer for the origin of deep-water masses, bear the fingerprint of a northern hemisphere source (εNd = −11.4 to −9.4) throughout the studied interval (Fig. 3g). Consequently, we argue that the low benthic $\delta^{13}C$ reflects local bottom water sourced from surface waters with a high nutrient concentration within the narrow, restricted North Atlantic basinal deep-water circulation. A probable nutrient source is 'fossil' carbon that leaks in from the Arctic Ocean and subarctic seas (Greenland and Norwegian Seas), which had high nutrient stocks during the Eocene because of their semi-isolation, heavily vegetated margins[24] and high riverine inflow[25–27].

We identify three circulation regimes based on our new Eocene–Oligocene proxy records and comparisons with published data (Figs. 2 and 3). Focusing first on $\delta^{13}C$ (Fig. 2), under Regime 1 (>35.8 Ma), SLS bottom waters were isolated from the rest of the Atlantic and a distinct NCW with a low $\delta^{13}C$ bathed Site 647. After ~35.8 Ma, an approximately 1.5–2 million-year-long (~35.8 to ~33.8 Ma) negative $\delta^{13}C$ excursion (0.5–1‰ VPDB $\delta^{13}C$ decrease) is seen to varying degrees at Sites 612, U1411 and 647, as well as some other Atlantic sites (1053, 1090 and 366). Offsets in this excursion's timing between sites are probably caused by age-model differences. Regime 2 encompasses the onset and peak of the $\delta^{13}C$ excursion. Importantly, the $\delta^{13}C$ excursions are largest (maximum 1‰ VPDB) at Sites 612 and U1411 sitting in the DWBC (Fig. 1). Although noted previously[28], the wider significance of this $\delta^{13}C$ excursion has not been fully explored. The observation that Sites 612 and U1411, directly downstream of Site 647, gain benthic $\delta^{13}C$ signals close to the SLS end member suggests that the signal was propagated from the north. Thus, it records the southward export of Arctic-imprinted, nutrient-rich NCW. The increase in Atlantic benthic $\delta^{13}C$ towards the end of Regime 2 indicates that either the pulse of NCW ended, or sufficiently ventilated surface water with a higher $\delta^{13}C$ was imported to the convection sites. Regime 3, described below, represents the phase during which a more mature form of NCW existed.

Deep-water cooling, salinification and destratification

A second prominent feature is the pattern of SLS benthic $\delta^{18}O$. The majority of the pre-Oligocene $\delta^{18}O$ data south of Site 647 ranged between 0.4 and 1.2‰ VPDB (Fig. 2). Strikingly, in the SLS during Regime 1, benthic $\delta^{18}O$ is 1–3‰ VPDB lower than that of the ensemble. The primary controls on benthic $\delta^{18}O$ are BWT and the $\delta^{18}O$ composition of seawater—the latter reflects the global glacial ice volume and local salinity. Assuming minimal ice before 34 Ma, the relatively low $\delta^{18}O$ in the SLS benthos indicates a considerably warmer or fresher water mass bathing the seafloor compared with southern stations. Benthic $\delta^{18}O$ from Sites 647 and 112 increased gradually from 36.0 to 35.4 Ma, then again from ~34.6 to 34.4 Ma, and had converged close to the dominant Atlantic trend by ~34.3 Ma, that is, coincident with or just lagging the Atlantic-wide $\delta^{13}C$ minimum. Diagenetic alteration of Site 647 benthic fossils[29] is ruled out because of (1) the excellent fossil calcite preservation[21] (Supplementary Information) and (2) the similarity of our new planktic $\delta^{18}O$ values from Sites 647 and U1411 (Fig. 3). Moreover, a similar pattern of decreasing benthic $\delta^{18}O$ is seen in a North Sea record[30], although at shallower depths (~500 m).

Mg/Ca BWT helps deconvolve the temperature and salinity influences on $\delta^{18}O$ (Methods and Supplementary Information). Across the EOT, Site 647 Mg/Ca data suggest a BWT cooling of ~1 °C combined with a ~0.6‰ VPDB increase in seawater $\delta^{18}O$ ($\delta^{18}O_{sw}$), in agreement with previous studies[31] (Fig. 3a). From this, we estimate a gradual bottom-water cooling in the SLS of ~3–4 °C between 37.5 Ma and 35 Ma, which is similar to the observed northern high-latitude sea-surface coolings[32]. Substituting the Mg/Ca BWTs into a $\delta^{18}O$ palaeotemperature equation (Methods) yields ice-free $\delta^{18}O_{sw}$ estimates of between −3 and −4‰ $\delta^{18}O$ during this interval. Based on these $\delta^{18}O_{sw}$ constraints, we estimated the late Eocene SLS bottom salinities using relevant modern $\delta^{18}O_{sw}$–sea surface salinity (SSS) relationships[33] (Fig. 3c).

Applying a modern SSS–$\delta^{18}O_{sw}$ relationship from eastern Greenland, today a conduit for low salinity (32 PSU (practical salinity units)) Arctic outflow implies a Site 647 bottom-water salinity of 30–32 PSU before 36 Ma, which increased by 2–3 PSU from 36 to 34 Ma. The salinity change is similar when a Laptev Sea (today fed by large Siberian rivers) $\delta^{18}O_{sw}$–salinity regression is applied. Although SSS–$\delta^{18}O_{sw}$ relationships are spatially widely variable, and modern relationships are only loose analogues for the Eocene, our inferred values are compatible with modern temperature–salinity fields. Therefore, we suggest that (1) before 36 Ma the SLS bottom waters were relatively fresh, and (2) SLS bottom salinity increased from Regime 1 to 2. This conclusion does not change even if samples older than 35 Myr are biased to higher Mg (Supplementary Information)

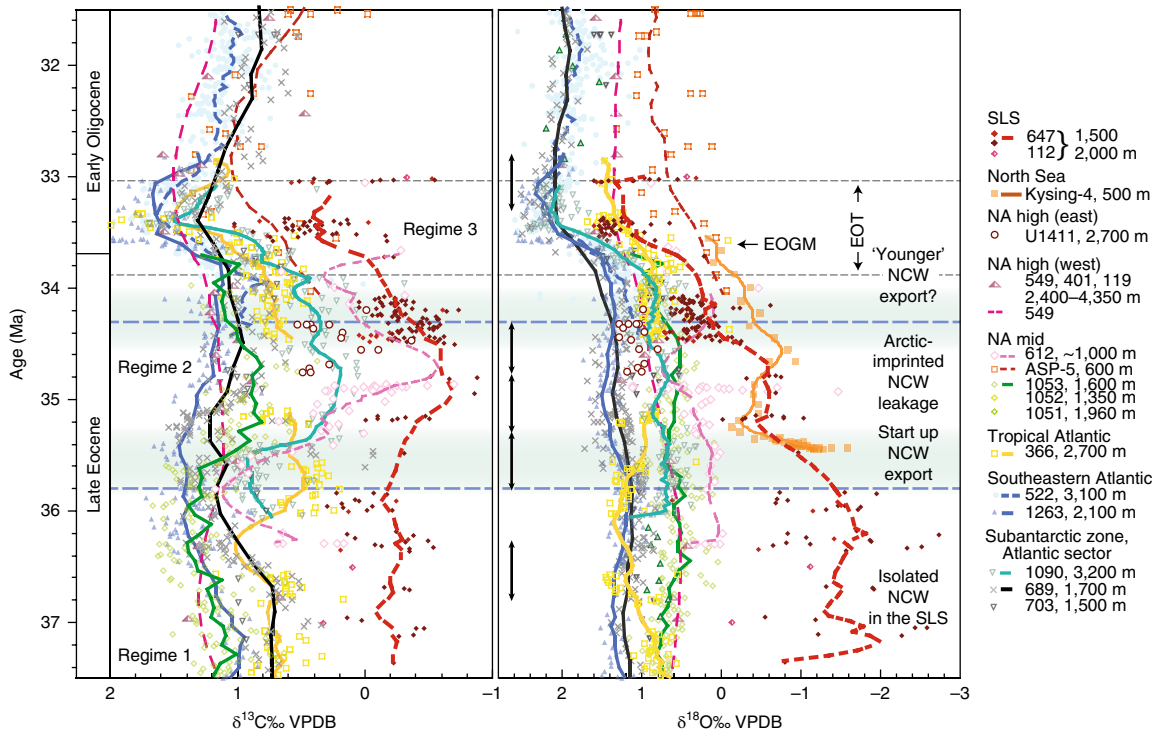

Fig. 2 | New and published Atlantic benthic $\delta^{18}O$ and $\delta^{13}C$ (*Cibicidoides* adjusted (Methods)). The EOT (fine dashed horizontal lines) and the EOGM event are identified by the step increase and maximum, respectively, in $\delta^{18}O$ in the earliest Oligocene. Trend lines represent smoothed curve fits that incorporate a geometric weighting. Regimes 1–3, separated by horizontal dashed blue lines, are phases of ocean circulation defined here based on proxy data. Pale aqua shading represents transition phases. Vertical black arrows identify the time windows gridded in Fig. 4. Supplementary Information gives the data sources, age modelling and an expanded figure with additional data. NA, North Atlantic; SLS, southern Labrador Sea.

because the salinity signal is embedded in the benthic $\delta^{18}O$, which is independent of Mg/Ca. This interpretation is consistent with that for pre-formed nutrients—they are both likely to have derived from the Arctic Ocean. Proxies and models agree that the Arctic had a thick freshwater cap during the Palaeogene as a consequence of a strong hydrological system and high fluvial inputs under greenhouse forcing, combined with restricted salt input[26,33–35]. With no Pacific Ocean outlet at this time, major surface discharge occurred through the Nordic Seas[34,36].

Site 647 planktic foraminifera $\delta^{18}O$ and $\delta^{13}C$ add information on the upper water column. The $\delta^{18}O$ of mixed-layer (surface) species is 1–2‰ VPDB lower than deep dwellers (subthermocline), consistent with a stratified upper ocean and calcification of mixed-layer dwellers high in the water column or during the warmest season (Fig. 3b). During Regime 1, and before 34.5 Ma, the $\delta^{18}O$ of the deep-dwelling planktic species is indistinguishable from benthic foraminifera, which reflects the influence of relatively fresh deep water at subthermocline levels in the SLS. Site 647 planktic data are sparse before 35 Ma due to the low foraminiferal abundance and coring gaps. However, after 34.5 Ma, deep-dwelling planktic and benthic $\delta^{18}O$ records separate coincident with the appearance of deep water with temperature and salinity properties similar to typical Atlantic values. Additionally, a progressive collapse in the planktic–benthic $\delta^{13}C$ gradient (Fig. 3d,e) is documented that captures the SLS water column transition from being well-stratified with large vertical $\delta^{13}C$ differences (1–1.5‰ VPDB) during Regime 1, to a state with a smaller $\delta^{13}C$ gradient (0.5‰ VPDB) comparable to the better-mixed modern North Atlantic convection sites[23] by ~34.3 Ma. Both observations are consistent with increasing NCW volume. An abrupt shift in Site 647 benthic assemblages at 34.3 Ma from agglutinated species tolerant of carbonate-poor, nutrient-rich environments, to calcareous species suited to a stronger current flow[37], coincident with other changes (Fig. 3f), provides further evidence for increased convection. Circulation Regime 3 begins at 34.3 Ma, when a saltier, denser form of NCW with a higher $\delta^{13}C$ is exported through the SLS.

Deep-water sources and sinking

Our Site 647 fish debris εNd data behave as a conservative tracer of northern sourced deep water (Supplementary Information) and can be compared with published ocean references[38,39] to identify the probable NCW source regions (Fig. 3g). Although we do not reconstruct Nd directly for Regime 1, our sample from 39 Ma is similar to the rest of the record, which implies that no systematic change in εNd and thus bottom-water provenance as NCW evolved. The comparison suggests that the Southern Ocean, which has the highest end-member εNd signature in our compilation, was not the source of bottom waters at Site 647. Moreover, we do not find evidence for the prominent EOT shift to high εNd values found in the Southern Ocean records[40]. Previous studies have suggested that, prior to deepening of the Greenland–Scotland Ridge (GSR), NCW was sourced from the Labrador Sea[10,13]. Modern Labrador Sea deep water, however, has characteristically low εNd (about −14), which reflects erosional inputs from the cratonic hinterland[41]. In contrast, Site 647 Nd is significantly more radiogenic (εNd = −11.4 to −9.4), and a closer match to the range of values measured in the Nordic Sea overflows (εNd of about −12.0 to −8.4) (refs [41,42]) and proximal Arctic Ocean basins above 500 m (εNd = −11.7 to −8.8) (ref. [43]). A Palaeogene presence of Tethys-sourced deep water at Site 647 is another possibility, as the Tethyian εNd signature (εNd = −10.0 to −9.3) (refs [44,45]) is indistinguishable from that of the North Atlantic water masses. However, palaeogeographic reconstructions suggest

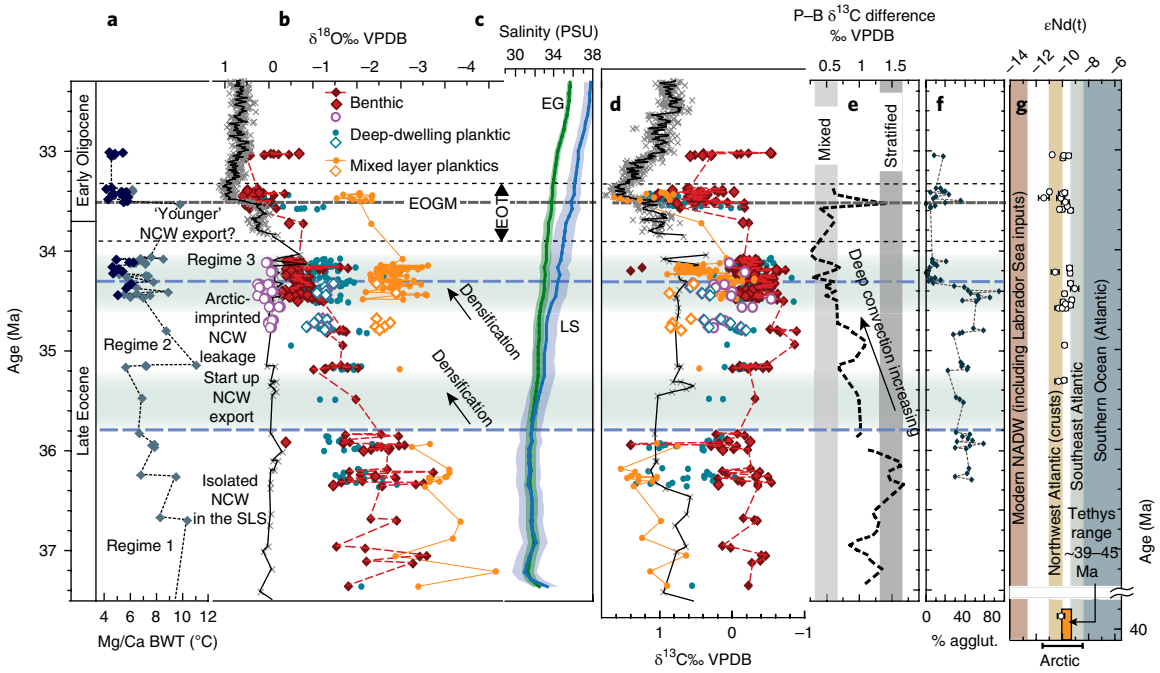

Fig. 3 | Sites 647 and U1411 multiproxy data. a, Mg/Ca BWT; paler blue symbols, maximum BWTs due to potential Fe contamination (Supplementary Information). **b**, Planktic and benthic $\delta^{18}O$ (black symbols, equatorial Pacific EOT chemostratigraphic data[22]; open symbols, U1411). **c**, Estimated Site 647 bottom-water salinity based on modern $\delta^{18}O_{sw}$ relationships (Methods). Error envelopes are based on 2 s.d. of the Mg/Ca BWT. LS, Laptev Sea; EG, eastern Greenland. **d**, Planktic and benthic $\delta^{13}C$ (symbols as in **b**). **e**, Site 647 planktic–benthic (P–B) $\delta^{13}C$ difference and modern gradients[23]. **f**, Site 647 agglutinated (agglut.) benthic foraminifera[37]. **g**, Site 647 fish tooth Nd and EOT ocean signatures, including Arctic ranges (error bars = 2σ standard reproducibility).

that water mass exchange between the European Tethys and Nordic Seas was limited during the middle-to-late Eocene[25,46], which makes this unlikely.

The only connections between the Arctic Ocean and Nordic Seas during the Palaeogene were shallow[27,46,47]. The transfer of freshened, nutrient-rich waters from the Arctic would have occurred via a proto Greenland Current. The similarity between the North Sea (Kysing-4 borehole) and Site 647 benthic $\delta^{18}O$, as well as independent evidence for low salinities in the Nordic Seas[34,48], is consistent with this picture. Transport from the subarctic seas to the Atlantic Ocean was also shallow, and the sinking of Arctic-imprinted NCW must have taken place south of the GSR until it subsided. With sufficient cooling in the subarctic seas, the density contrast of brackish Arctic waters with warmer saltier North Atlantic surface waters permitted sinking, which resulted in the distinct bottom water recorded at Site 647.

Importantly, before ~36 Ma, Arctic-imprinted NCW deep-water formation was minimal, which implies a regular stratification and stagnation in the SLS. This is consistent with the considerable noise in $\delta^{13}C$ and $\delta^{18}O$ during Regime 1. How this deep water remained isolated in the SLS at depths of around 2,000 m under Regime 1 remains uncertain. One possibility is that production and export rates of local deep waters in the North Atlantic were high compared with the influx of southern-sourced deep waters, and subsequently increased further as the cooler, saltier NCW started to be produced. Alternatively, bathymetric highs associated with the now-extinct Labrador Sea spreading ridges and the West Thulean igneous province to the south may have isolated the SLS subsurface waters from the overall Atlantic during the early Palaeogene[7]. In this case, the cessation of Labrador Sea spreading close to the EOT was probably important, as it allowed ridges to subside and enabled an enhanced deep-water export.

We illustrate the isotopic evidence and sequence of EOT oceanic changes using natural neighbour regridding (Methods) of compiled isotopic data to produce south–north Atlantic depth transects during time windows centred on circulation Regimes 1–3 (Fig. 4; Supplementary Information gives data sources, additional transects and maps). Before ~36 Ma (Regime 1), a strong isotopic $\delta^{18}O$ and $\delta^{13}C$ depletion affects water masses down to ~2,000 m above 40° N (Fig. 4a,b), which corresponds to small amounts of low salinity, high-nutrient Arctic-imprinted NCW in the SLS. The rest of the Atlantic is filled with deep waters with a more homogeneous $\delta^{18}O$ sourced from southerly and possibly low-latitude regions[10,13]. Increasing subarctic $\delta^{18}O$, which reflects progressive salinification and densification of Nordic surface waters, is accompanied by a 0.5–1.0 Myr pulse of NCW export during Regime 2 (Fig. 4c–h). By 33.3–34.3 Ma the 'fresh' SLS deep-water signal no longer exists, bottom-water $\delta^{13}C$ has increased, the acute phase of low $\delta^{13}C$ export is over and a better-ventilated NCW is exported (Regime 3). Importantly, the initial pulse of NCW export under Regime 2 is recorded by decreasing $\delta^{13}C$ signals in deep waters down stream of the SLS. The presence of late Eocene NCW in the Atlantic was not identified in previous $\delta^{13}C$ records[10,13,20] because NCW was assumed to have a high $\delta^{13}C$ signature similar to that of modern NADW.

Causes and consequences of NCW export

Deepening of the GSR in the late Eocene, for which there is geological evidence[4,34], would have increased the Nordic overflows, and thus strengthened NCW production. Modelling suggests that deepening of the GSR below a crtical depth of 50 m initiates a threshold switch from lagoonal to estuarine circulation that salinifies the Nordic Seas sufficiently to intensify the northern deep-water production[34]. Although this idea is consistent with our findings,

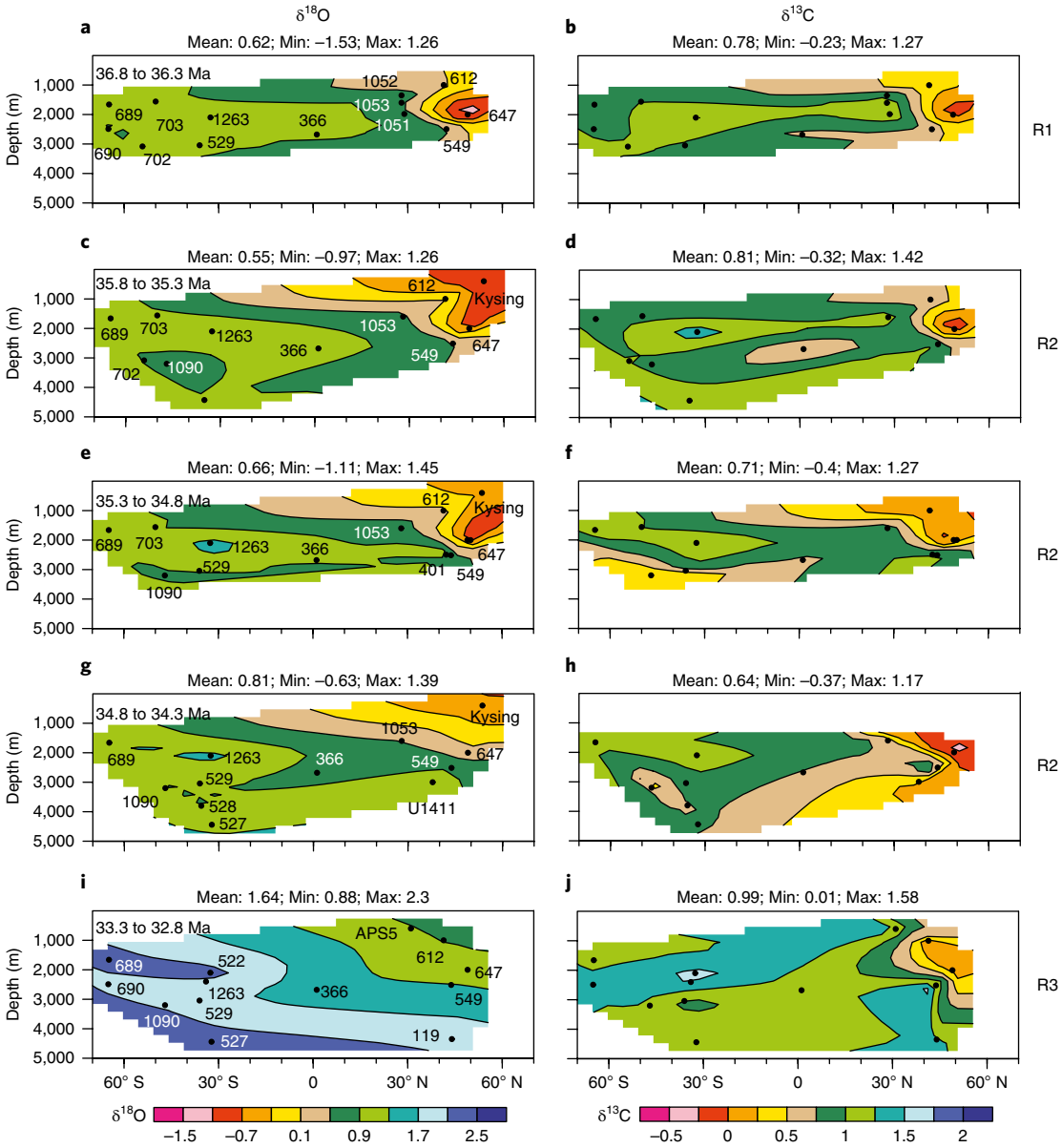

Fig. 4 | Depth–latitude compilation of Atlantic benthic $\delta^{13}C$ and $\delta^{18}O$ during the late Eocene to early Oligocene, constructed using natural neighbour interpolation. a–j, Data are plotted at their 34-Myr-old positions (dots indicate core palaeopositions). The five time slices illustrate the transition through the three circulation regimes in Fig. 2: R1, Regime 1 (**a** and **b**); R2, Regime 2 (**c**–**h**); R3, Regime 3 (**i** and **j**). The Supplementary Information gives the data sources and a more extensive set of gridded time slices and late Eocene maps.

the bathymetric history of the GSR is currently too crude to date such a change accurately. Moreover, we propose that contemporaneous restrictions to the Arctic–Nordic Sea exchange also played a role. Geological evidence suggests that the Barents Sea–Arctic passageway shoaled in the latest Eocene[46,47] and that relative sea-level variations in the Arctic were decoupled from global trends from the late Eocene to the early Miocene[49]. This palaeogeographic Arctic isolation enhanced the salinification in the Nordic Seas as brackish Arctic outflows were gradually cut off.

Changes in the NCW production had varied and competing effects. Its onset presumably impacted poleward heat transport in both hemispheres[17,18]. The initial export of nutrient-rich, Arctic-imprinted NCW may have generated a short-lived pulse of CO_2, on the order of 100–200 ppm, which is consistent with proxy compilations that show a temporary reversal in the falling CO_2 trend between ~34 to ~35 Ma (ref. [50]). On the other hand, a strengthening NCW production and an enhanced northward ocean heat transport could have played a role in longer-term CO_2 drawdown due to an accompanying increase in rainfall over land and associated CO_2-weathering feedbacks[16]. The circulation change timing, 1–2 million years prior to Antarctic glaciation, reinforces the idea that the onset of NCW played a role in preconditioning the late Eocene Earth system for the greenhouse-to-icehouse transition.

Methods

Methods, including statements of data availability and any associated accession codes and references, are available at https://doi.org/10.1038/s41561-018-0069-9

Received: 30 July 2017; Accepted: 22 January 2018;
Published online: 26 February 2018

References

1. Broecker, W. S. Paleocean circulation during the last deglaciation: a bipolar seesaw? *Paleoceanography* **13**, 119–121 (1998).
2. de Boer, A. M., Toggweiler, J. R. & Sigman, D. M. Atlantic dominance of the meridional overturning circulation. *J. Phys. Oceano.* **38**, 435–450 (2008).
3. Toggweiler, R. & Samuels, B. Effect of Drake Passage on the global thermohaline circulation. *Deep Sea Res. I* **42**, 477–500 (1995).
4. Abelson, M. & Erez, J. The onset of modern-like Atlantic meridional overturning circulation at the Eocene–Oligocene transition: evidence, causes, and possible implications for global cooling. *Geochem. Geophys. Geosystems* **18**, 2177–2199 (2017).
5. Cramer, B. S., Toggweiler, J. R. T., Wright, J. D., Katz, M. E. & Miller, G. H. Ocean overturning since the Late Cretaceous: inferences from a new benthic foraminiferal isotope compilation. *Paleoceanography* **24**, PA4216 (2009).
6. Davies, R., Cartwright, J., Pike, J. & Line, C. Early Oligocene initiation of North Atlantic Deep Water formation. *Nature* **410**, 917–920 (2001).
7. Egloff, J. & Johnson, G. L. Morphology and structure of the Southern Labrador Sea. *Can. J. Earth Sci.* **12**, 2111–2133 (1975).
8. Miller, K. G. & Tucholke, B. E. in *Structure and Development of the Greenland–Scotland Ridge* (eds Bott, M. H. P., Thiede, J., Saxov, S. & Talwani, M.) 549–589 (Plenum, New York, 1983).
9. Via, R. K. & Thomas, D. J. Evolution of Atlantic thermohaline circulation: early Oligocene onset of deep-water production in the North Atlantic. *Geology* **34**, 441–444 (2006).
10. Borrelli, C., Cramer, B. S. & Katz, M. E. Bipolar Atlantic deepwater circulation in the middle–late Eocene: effects of Southern Ocean gateway openings. *Paleoceanography* **29**, 308–327 (2014).
11. Boyle, P. R. et al. Cenozoic North Atlantic deep circulation history recorded in contourite drifts, offshore Newfoundland, Canada. *Mar. Geol.* **385**, 185–203 (2017).
12. Hohbein, M. W., Sexton, P. F. & Cartwright, J. A. Onset of North Atlantic Deep Water production coincident with inception of the Cenozoic global cooling trend. *Geology* **40**, 255–258 (2012).
13. Langton, S. J., Rabideaux, N. M., Borrelli, C. & Katz, M. E. Southeastern Atlantic deep-water evolution during the late–middle Eocene to earliest Oligocene (Ocean Drilling Program Site 1263 and Deep Sea Drilling Project Site 366). *Geosphere* **12**, 1032–1047 (2016).
14. Wright, J. D. & Miller, K. G. Control of North Atlantic Deep Water circulation by the Greenland–Scotland Ridge. *Paleoceanography* **11**, 157–170 (1996).
15. Sijp, W. P., England, M. H. & Huber, M. Effect of the deepening of the Tasman Gateway on the global ocean. *Paleoceanography* **26**, PA4207 (2011).
16. Elsworth, G., Galbraith, E., Halverson, G. & Yang, S. Enhanced weathering and CO_2 drawdown caused by latest Eocene strengthening of the Atlantic meridional overturning circulation. *Nat. Geosci.* **10**, 213–216 (2017).
17. Tigchelaar, M., von der Heydt, A. S. & Dijkstra, H. A. A new mechanism for the two-step $\delta^{18}O$ signal at the Eocene–Oligocene boundary. *Clim. Past.* **7**, 235–247 (2010).
18. Zhang, Z. et al. Tropical seaways played a more important role than high latitude seaways in Cenozoic cooling. *Clim. Past.* **7**, 801–813 (2011).
19. Huber, M. & Sloan, L. C. Heat transport, deep waters, and thermal gradients: coupled simulation of an Eocene greenhouse climate. *Geophys. Res. Lett.* **28**, 3481–3484 (2001).
20. Pusz, A. E., Thunell, R. C. & Miller, K. G. Deep water temperature, carbonate ion, and ice volume changes across the Eocene–Oligocene climate transition. *Paleoceanography* **26**, PA2205 (2011).
21. Firth, J. V., Eldrett, J. S., Harding, I. C., Coxall, H. K. & Wade, B. Integrated biomagnetochronology for the Palaeogene of ODP Hole 647A: implications for correlating palaeoceanographic events from high to low latitudes. *Geol. Soc. Spec. Pub.* **373**, 29–78 (2013).
22. Coxall, H. K. & Wilson, P. A. Early Oligocene glaciation and productivity in the eastern equatorial Pacific; insights into global carbon cycling. *Paleoceanography* **26**, PA2221 (2011).
23. Kroopnick, P. The distribution of ^{13}C of $\sum CO_2$ in the world oceans. *Deep Sea Res.* **32**, 57–84 (1985).
24. Golovneva, L. B. Early Palaeogene floras of Spitsbergen and North Atlantic floristic exchange. *Acta Univ. Carol. Geol.* **44**, 39–50 (2000).
25. Akhmetiev, M. A. & Beniamovski, V. N. Paleogene floral assemblages around epicontinental seas and straits in Northern Central Eurasia: proxies for climatic and paleogeographic evolution. *Geol. Acta* **7**, 297–309 (2009).
26. Gleason, J. D. et al. Early to middle Eocene history of the Arctic Ocean from Nd–Sr isotopes in fossil fish debris, Lomonosov Ridge. *Paleoceanography* **24**, PA2215 (2009).
27. O'Regan, A. M., Williams, C. J., Frey, K. E. & Jakobsson, M. A synthesis of the long-term paleoclimatic evolution of the Arctic. *Oceanography* **24**, 66–80 (2011).
28. Pusz, A. E. et al. Stable isotopic response to late Eocene extraterrestrial impacts. *Geol. Soc. Am. Special Papers* **452**, 83–95 (2009).
29. Arthur, M. A. *et al.* in *Proc. Ocean Drilling Program Scientific Results* Vol. 105 (eds Srivastava, S. P. et al.) 111–135 (Ocean Drilling Program, 1989).
30. Nielsen, S. B. et al. The evolution of western Scandinavian topography: a review of Neogene uplift versus the ICE (isostasy–climate–erosion) hypothesis. *J. Geodynam.* **47**, 72–95 (2009).
31. Lear, C. H., Bailey, T. R., Pearson, P. N. P., Coxall, H. K. & Rosenthal, Y. Cooling and ice growth across the Eocene–Oligocene transition. *Geology* **36**, 251–254 (2008).
32. Liu, L. et al. Global cooling during the Eocene–Oligocene climate transition. *Science* **323**, 1187–1190 (2009).
33. Waddell, L M. & Moore, T. C. Salinity of the Eocene Arctic Ocean from oxygen isotope analysis of fish bone carbonate. *Paleoceanography* **23**, PA1S12 (2008).
34. Stärz, M., Jokat, W., Knorr, G. & Lohmann, G. Threshold in North Atlantic–Arctic Ocean circulation controlled by the subsidence of the Greenland–Scotland Ridge. *Nat. Commun.* **8**, 15681 (2017).
35. Roberts, C. D., LeGrande, A. N. & Tripati, A. K. Climate sensitivity to Arctic seaway restriction during the early Paleogene. *Earth Planet. Sci. Lett.* **286**, 576–585 (2009).
36. Brinkhuis, H. et al. Episodic fresh surface waters in the Eocene Arctic Ocean. *Nature* **441**, 606–609 (2006).
37. Kaminski, M. & Ortiz, S. The Eocene–Oligocene turnover of deep-water agglutinated foraminifera at ODP Site 647, Southern Labrador Sea (North Atlantic). *Micropaleontology* **60**, 53–66 (2014).
38. Burton, K. W., Ling, H. F. & O'Nions, R. K. Closure of the Central American isthmus and its effect on deep-water formation in the North Atlantic. *Nature* **386**, 382–385 (1997).
39. O'Nions, R. K., Frank, M., von Blanckenburg, F. & Ling, H. F. Secular variation of Nd and Pb isotopes in ferromanganese crusts from the Atlantic, Indian and Pacific Oceans. *Earth Planet. Sci. Lett.* **155**, 15–28 (1998).
40. Scher, H. D. & Martin, E. E. Timing and climatic consequences of the opening of Drake Passage. *Science* **312**, 428–430 (2006).
41. Lambelet, M. et al. Neodymium isotopic composition and concentration in the western North Atlantic Ocean: results from the GEOTRACES GA02 section. *Geochem. Cosmochim. Acta* **177**, 1–29 (2016).
42. Lacan, F. & Jeandel, C. Acquisition of the neodymium isotopic composition of the North Atlantic Deep Water. *Geochem. Geophys. Geosystems* **6**, Q1208 (2005).
43. Porcelli, D. et al. The distribution of neodymium isotopes in Arctic Ocean basins. *Geochim. Cosmochim. Acta* **73**, 2645–2659 (2009).
44. Grandjean, P., Cappetta, H., Michard, A. & Albarede, F. The assessment of REE patterns and $^{143}Nd/^{144}Nd$ Nd ratios in fish remains. *Earth Planet. Sci. Lett.* **84**, 181–196 (1987).
45. Stille, P. & Fischer, H. Secular variation in the isotopic composition of Nd in Tethys seawater. *Geochim. Cosmochim. Acta* **54**, 3139–3145 (1990).
46. Kharin, G. S. & Lukashina, N. P. Paleogeography of the Norwegian–Greenland and northwestern European Sea basins in the Paleogene. *Oceanology* **50**, 226–239 (2010).
47. Musatov, E. E. & Pogrebitskij, Y. E. Late Mesozoic–Cenozoic evolution of the Barents Sea and Kara Sea continental margins. *Polarforschung* **68**, 283–290 (2000).
48. Andreasson, F. P., Schmitz, B. & Spiegler, D. Stable isotopic composition (delta$^{18}OCO_3^{2-}$, delta^{13}C) of early Eocene fish-apatite from Hole 913B: an indicator of the early Norwegian–Greenland Sea paleosalinity. In *Proc. Ocean Drilling Program Sci. Res.* Vol. 151 (eds Thiede, J. et al.) 583–591 (Ocean Drilling Program, 1996).
49. Hegewald, A. & Jokat, W. Relative sea level variations in the Chukchi region — Arctic Ocean — since the late Eocene.*Geophys. Res. Lett.* **40**, 2013 (2013).
50. Anagnostou, E. et al. Changing atmospheric CO_2 concentration was the primary driver of early Cenozoic climate. *Nature* **533**, 380–384 (2016).

Acknowledgements

Samples were provided by the International Ocean Discovery Program (IODP), which includes the predecessors the International Ocean Drilling Program (IODP), Deep Sea Drilling Project (DSDP) and Ocean Drilling Program (ODP). We thank J. Becker and M. Spencer for technical assistance with the stable isotopes, and H. Öste and E. Axelsson for preparing the core samples. H.K.C. was supported by a Royal Society Research Fellowship, Swedish Funding agency (VR) no. DNR 2008-2859 and the Bolin Centre for Climate Research, and T.vdF. by NERC Grants NE/I006257/1 and NE/L004607/1. K.K.S. acknowledges financial support from the Danish Council for Independent Research/Natural Sciences (DFF/FNU; Grant 11-107497).

Author contributions

H.K.C. and J.B. conceived the project. H.K.C. directed the research, generated the stable isotope data for Sites 112, 647 and U1411, compiled the proxy records and led writing of the paper. A.L.-L. produced the new Site 612 data and age model. C.H.L. conducted the trace metal analysis. C.E.H. produced and interpreted the Nd data with the help of

T.vdF. M.O. produced the palaeogeographic map for Fig. 1 and conducted the subsidence modelling. K.K.S. helped produce the Site 647 age model. M.H. helped with the interpretative framework and produced the interpolated Atlantic depth isotopic transects and maps. J.C.Z. and A.M.d.B. helped interpret the data. All of the authors contributed to writing the manuscript.

Competing interests
The authors declare no competing interests.

Additional information
Supplementary information is available for this paper at https://doi.org/10.1038/s41561-018-0069-9.

Correspondence and requests for materials should be addressed to H.K.C.

Methods

Palaeogeographic plate reconstructions and modern Atlantic Ocean circulation inset. The palaeogeographic plate reconstructions used to produce Fig. 1 were performed using G-plates, with coastlines adapted from E–O reconstructions (34 Ma) of R. Blakey, Colorado Plateau Geosystems. The inset figure showing modern North Atlantic surface- and deep-current paths is based on the schematics of Schmitz and McCartney[51].

Age framework. The age control for Site 647 is based on biomagnetostratigraphy[21], adjusted here using Site 647 $\delta^{18}O$ chemostratigraphy (Supplementary Information gives further details for Site 647 and the other sites). Site 112 ages are estimated from biostratigraphy[52]. Site U1411 ages are based on IODP Experiment 342 shipboard magnetostratigraphy[53]. The Site 612 age model is based on the biostratigraphy of Miller and Katz[54]. In all cases, datum events are calibrated or rescaled using linear interpolation to the chronology of Cande and Kent[55] to permit comparison with the Atlantic benthic isotope stack[5,56,57], much of which exists on this common timescale.

Stable isotopes. Planktic and benthic foraminifera are present throughout the EOT interval of Sites 647, 112 and U1411, although heavily diluted by terrestrial clay. Planktic and benthic foraminifera are somewhat more common at Site 612. Tests are exceptionally well preserved at all sites throughout the studied intervals (Supplementary Information for further details).

Foraminiferal $\delta^{18}O$ and $\delta^{13}C$ for Sites 647 and 112 were derived from the benthic foraminifera taxa *Oridorsalis umbonatus* (shallow infaunal) and *Cibicidoides* spp. (epifaunal), where available, both shown to be a reliable deep-sea tracer in previous studies[22,58] (Supplementary Information). Site U1411 measurements are on *Cibicidoides* spp. and the new Site 612 measurements on *Hanzawaia ammophila*. Sites 647 and U1411 planktic foraminiferal analyses were made on *Turborotalia ampliapertura* and *Catapsydrax unicavus*, which represent the surface mixed layer and thermocline/subthermocline habitats, respectively[59]. Site 647 stable isotope analysis was performed at Cardiff University using a ThermoFinnigan MAT252 mass spectrometer equipped with an automated KIEL III carbonate preparation unit. Additional samples were run at the National Oceanographic Centre, Southampton University, using a Europa Geo 20–20 mass spectrometer equipped with a CAPS automatic carbonate preparation system. The standard external analytical precision quoted at Cardiff was better than 0.05‰ for $\delta^{18}O$ and 0.03‰ for $\delta^{13}C$, and ±0.08‰ for $\delta^{18}O$ and $\delta^{13}C$ at Southampton. Site 612 analyses were measured at the Department of Geological Sciences, Stockholm University, on a ThermoFinnigan MAT 252 IRMS coupled with a Finnigan Gasbench II device. The standard external analytical precision, based on replicate analysis of in-house standards calibrated to international standards (NBS19, IAEA-CO-1 and IAEA-CO-8), was better than 0.07‰ for $\delta^{13}C$ and 0.15‰ for $\delta^{18}O$. All the results are reported relative to the VPDB standard. Our Site 647 *O. umbonatus* data were adjusted to *Cibicidoides* values (believed to be close to ambient seawater) by subtracting −0.28‰ for the $\delta^{18}O$ (ref. [60]), and by the3 addition of 1.4‰ to the $\delta^{13}C$ (ref. [61]) (consistent with a species -comparison study in a restricted basin in the western North Pacific, which closely matches our few Site 647 *Cibicidoides*–*O. umbonatus* $\delta^{13}C$ pairs). The different species are differentiated in Figs. 2 and 3 by dark red (*O. umbontatus*) and bright red (*Cibicidoides* spp.) symbols. For Site 612 the following adjustments[60] were used when integrating the new *H. ammophila* data: $(\delta^{18}O_{H.\ ammophila} - 0.16)/0.62 = \delta^{18}O_{Cibicidoides}$, and $\delta^{13}C_{H.\ ammophila} + 0.08 = \delta^{13}C_{Cibicidoides}$. The planktic–benthic $\delta^{13}C$ gradient ($\Delta\delta^{13}C$) was generated by resampling the planktic and benthic foraminifera $\delta^{13}C$ curves to provide paired samples. Our new $\delta^{18}O$ and $\delta^{13}C$ are compared with 21 other Atlantic data sets that build on other compilations[5,57]. The new data produced in this study are presented in Supplementary Data File 1. Supplementary Table 1 gives the full list of site meta data and sources used in our Atlantic compilation.

Trace-metal analysis and Mg/Ca foraminiferal bottom-water palaeothermometry. Trace-metal content (Mg/Ca, Mn/Ca, Fe/Ca) was analysed on Site 647 *O. umbonatus*. Prior to the analysis, benthic foraminifera samples were cleaned following the protocol of Boyle and co-workers[62,63] without the reducing step due to the scarcity of material, but including contaminant removal under binocular microscope after the oxidative step[64]. The samples were subjected to one weak acid leach prior to dissolution and dilution. The analysis was carried out at Cardiff University on a Thermo Element XR ICP-MS against standards with equivalent Ca concentrations. Multi-element standards were made in-house from single element standards supplied by Greyhound Chromatography and Allied Chemicals. The analytical precisions determined from separate consistency standards over the course of a year are 0.5% for Mg/Ca, and 2% for Mn/Ca and Fe/Ca (relative standard deviation). Mg/Ca palaeo-BWTs were calculated using an exponential calibration[58] (Supplementary Information and Supplementary Data File 2).

Our *O. umbonatus* Mg/Ca record is noisy and high Mg/Ca ratios are often associated with high Fe/Ca (correlation coefficient $r^2 = 0.4$) (Supplementary Data File 2). By excluding the samples with Fe/Ca » 900 µmol mol^{-1}, r^2 was reduced to 0.18. The subset of data with a lower Fe/Ca, largely the upper portion of the core in samples younger than 34.5 Myr (Supplementary Table 4), may be regarded as the most reliable. However, despite the higher Fe/Ca in the older samples, we believe the Mg/Ca data from the lower part of the core are not entirely flawed because the Fe/Ca versus Mg/Ca r^2 value based on the full sample set is still relatively low and there is overlap of Mg/Ca values with both high and low Fe/Ca around the EOT (Fig. 3a, paler blue symbols). Thus, the older Mg/Ca should provide realistic palaeo bottom-water temperatures (within the uncertainties of the method), and are thus included in the downcore record to provide ballpark BWTs and allow salinity reconstructions in the initial part of the late Eocene.

Bottom-water-salinity reconstruction. The pattern of progressive benthic $\delta^{18}O$ increase and maximum 4°C BWT cooling between 37.5 and 35.5 Ma implies that $\delta^{18}O_{sw}$ was changing over this period. To explore this further, bottom-water palaeosalinity was reconstructed based on modern SSS–$\delta^{18}O$ relationships. This was performed in two steps. First, $\delta^{18}O_{sw}$ values were calculated by substituting the Site 647 Mg/Ca BWTs into a $\delta^{18}O$-benthic foraminifera palaeotemperature equation[65]. Due to the noise in our estimated benthic BWTs, we used broad 'BWT brackets', based on mean BWT values for three intervals (Supplementary Table 5).

Second, bottom-water palaeosalinity was reconstructed based on the modern surface salinity $\delta^{18}O$ relationships for the Laptev Sea and East Greenland Current[66,67], regions with relatively low $\delta^{18}O_{sw}$ linked to the Arctic Ocean and Arctic outflows, respectively (the Laptev Sea is an Arctic shelf sea that receives large volumes of river runoff from Siberian rivers (22–34 PSU), whereas the East Greenland Current carries low salinity surface waters (32 PSU) out of the Arctic Ocean). It was assumed that these relationships remained the same downcore.

Laptev Sea[66]: $\text{salinity} = (\delta^{18}O_{sw} - 18.86) = 0.5 \quad R^2 = 0.98$

East Greenland[67]: $\text{salinity} = (\delta^{18}O_{sw} - 35.02) = 1.01$

The resulting curve, which is plotted as a 'smoothed curve-fit' in KaleidaGraph with error envelopes that represent limits determined by 2σ of the BWT brackets (Fig. 3c), provides coarse constraints on the evolution of Site 647 bottom-water salinity in the late Eocene. As discussed above, it is possible that the decreasing Mg/Ca between 37.5 and 35.5 Ma represents a decreasing trace-metal contamination rather than bottom-water cooling. If this is the case, then the BWTs around 37 Ma are too high, which would bias the salinities to values that are too salty. Thus, to include or exclude the older Mg/Ca data does not change the conclusions. We have confidence in the Mg/Ca after 34 Ma and thus have $\delta^{18}O_{sw}$ constrained there. The important point is that the subsurface densification signal is seen in the benthic foraminifera $\delta^{18}O$ record (increasing $\delta^{18}O$ from 37.5 to 35.5 Ma). It is impossible that this is an artefact of the Mg/Ca data.

Neodymium isotope methodology. Fish teeth and bone debris were hand-picked from the >63 µm fraction of sieved sediment and cleaned to remove adhering debris. The initial experiments (Supplementary Information) indicated that the 'simple cleaning method'[68] was sufficient. All the samples were dissolved in 2 M HCl, dried and converted into nitrate form prior to column chemistry. A standard two-stage ion chromatography procedure was used, which first isolated the rare-earth elements (REEs) from the sample matrix using TRU Spec resin (100–120 µm bead size) and then separated Nd from the other REEs with Ln-Spec resin (50–100 µm bead size)[69]. Neodymium isotope ratios were measured on a Nu Plasma MC-ICP-MS at Imperial College London in static mode. Instrumental mass bias was corrected for using a $^{146}Nd/^{144}Nd$ ratio of 0.7219. Samarium interference can be adequately corrected if the ^{144}Sm signal contributes less than 0.1% of the ^{144}Nd signal. The Sm contribution in all our samples was well below this level. Chemistry blanks were consistently below 10 pg Nd. Replicate analyses of the Nd standard JNdi yielded $^{143}Nd/^{144}Nd$ ratios from 0.512060 ± 0.000015 to 0.512251 ± 0.000015 ($n = 116$), dependent on the daily running conditions over 12 months. The external reproducibility of our chemistry and mass spectrometry procedure was monitored using a fossil-bone composite standard supplied by C. Trueman (University of Southampton), which yielded a $^{143}Nd/^{144}Nd$ ratio of 0.512377 ± 0.000028 ($n = 8$ over 18 months) and agrees, within error, with previously published values[70,71]. The standard material was digested for analysis following specific methods[70] for analytical consistency. Briefly, 50 mg of material was digested in 3 M HNO_3 in a Teflon beaker at 130 °C. Any material that remained after this step was subjected to a further 48 h digestion in a 3:1 mixture of 15 M HNO_3 to 27 M HF. To correct for the decay of ^{147}Sm to ^{143}Nd within the fish teeth over time, we used REE concentrations obtained in two samples from this site. The derived $^{147}Sm/^{143}Nd$ ratios of 0.129 and 0.134 are consistent with values reported in other studies[72–74]. We applied an average value of our measurements ($^{147}Sm/^{143}Nd = 0.132$) to all the remaining samples. All Nd isotope ratios are reported in epsilon notation (εNd) (Supplementary Table 6). The comparative εNd data in Fig. 3 are listed in Supplementary Table 7.

Atlantic isotopic depth sections. We used standard techniques in ocean data assimilation to create homogenized and interpolated maps of isotopic values based on the sparse data (Supplementary Table 1 gives site information, data sources and a more complete set of maps (Supplementary Fig. 9). For the transects, the proxy data were placed on a regular latitude–depth grid based on their reconstructed depths and palaeolocations, and the natural neighbour regridding routines

implemented in the NCAR Command Language were used to create interpolated, gridded values (www.ncl.ucar.edu/Document/Functions/Built-in/natgrid.shtml). Extrapolation beyond the convex hull of the kernel was not used. The background palaeogeography is based on a hotspot reference frame[75]. The differences in interpretation for our paper using the alternative Palaeomag reference frame described in the same study are negligible.

For the maps, the proxy records were interpolated using the technique of Barnes–Cressman iterated objective analysis implemented in the NCAR Command Language (www.ncl.ucar.edu/Document/Functions/Contributed/obj_anal_ic_Wrap.shtml). In this approach, each observation is assigned a circular radius of influence, *R*. Here we used successive values of *R* of 9°, 8°, 6°, 4°, 2° and 1°. A first guess of the value at every grid point was made by including all the observations within the region of influence of that grid point. A distance-weighted average of the differences between the first-guess fields and the actual observations was made, and this anomaly was added into the first-guess fields to calculate a second-guess field. Thus, observations from beyond the radius of influence were ignored in updating the field, and other observations closer to the initial observation were given greater weight. This was done for all grid points under consideration. The resulting fields were used as the basis for the next iteration, which was carried out with a smaller region of influence.

Data availability. The authors declare that lists of the sources of previously published data used in this study are available within the article and its Supplementary Information files. The new data are available at the Bolin Centre for Climate Research Database: http://bolin.su.se/data/Coxall-2018.

References

51. Schmitz, W. J. & McCartney, M. S. On the North Atlantic Circulation. *Rev. Geophys.* **31**, 29–49 (1993).
52. Laughton, A. S. et al. Shipboard reports of Sites 112, 118 and 119. In *Initial Rep. Deep Sea Dril. Project* Vol. 12 (eds Laughton, A. S. et al.) 161–253 (US Government Printing Office, Washington, 1972).
53. Norris, R. D. et al. In *Proc. Integrated Ocean Drilling Program* Vol. 342 (Integrated Ocean Drilling Program, 2014).
54. Miller, K. G. & Katz, M. E. Eocene benthic foraminiferal biofacies of the New Jersey Transect. In *Initial Rep. Deep Sea Drill. Project* Vol. 95 (eds Poag, C. W. et al.) 267–298 (US Government Printing Office, Washington, 1987).
55. Cande, S. C. & Kent, D. V. Revised calibration of the geomagnetic polarity timescale for the Late Cretaceous and Cenozoic. *J. Geophys. Res.* **100**, 6093–6095 (1995).
56. Zachos, J. C., Pagani, M., Sloan, L. C., Thomas, E. & Billups, K. Trends, rhythms, and aberrations in global climate 65 Ma to present. *Science* **292**, 686–693 (2001).
57. Zachos, J. C., Dickens, G. R. & Zeebe, R. E. An early Cenozoic perspective on greenhouse warming and carbon-cycle dynamics. *Nature* **451**, 279–283 (2008).
58. Lear, C. H. et al. Neogene ice volume and ocean temperatures: insights from infaunal foraminiferal Mg/Ca paleothermometry. *Paleoceanography* **30**, 1437–1454 (2015).
59. Pearson, P. N. et al. Warm tropical sea surface temperatures in the Late Cretaceous and Eocene epochs. *Nature* **413**, 481–487 (2001).
60. Katz, M. E. et al. Early Cenozoic benthic foraminiferal isotopes: species reliability and interspecies correction factors. *Paleoceanography* **18**, 1024 (2003).
61. Rathburn, A. E., Corliss, B. H., Tappa, K. D. & Lohmann, K. C. Comparisons of the ecology and stable isotopic compositions of living (stained) benthic foraminifera from the Sulu and South China Seas. *Deep Sea Res. I* **43**, 1617–1646 (1996).
62. Boyle, E. A. Manganese carbonate overgrowths on foraminifera tests. *Geochim. Cosmochim. Acta* **47**, 1815–1819 (1983).
63. Boyle, E. A. & Keigwin, L. D. Comparison of Atlantic and Pacific paleochemical records for the last 215,000 years: changes in deep ocean circulation and chemical inventories. *Earth Planet. Sci. Lett.* **76**, 135–150 (1985).
64. Barker, S., Greaves, M. & Elderfield, H. A study of cleaning procedures used for foraminiferal Mg/Ca paleothermometry. *Geochem. Geophys. Geosystems* **4**, 8407 (2003).
65. Marchitto, T. M. et al. Improved oxygen isotope temperature calibrations for cosmopolitan benthic foraminifera. *Geochim. Cosmochim. Acta* **130**, 1–11 (2014).
66. Mueller-Lupp, T., Erlenkueser, H. & Bauch, H. A. Seasonal and interannual variability of Siberian river discharge in the Laptev Sea inferred from stable isotopes in modern bivalves. *Boreas* **32**, 292–303 (2003).
67. Fairbanks, R. G., Charles, C. D. & Wright, J. D. *Radiocarbon After Four Decades* 473–500 (Springer, New York, 1992).
68. Martin, E. E. & Haley, B. A. Fossil fish teeth as proxies for seawater Sr and Nd isotopes. *Geochim. Cosmochim. Acta* **64**, 835–847 (2000).
69. Pin, C. & Zalduegui, J. S. Sequential separation of light rare-earth elements, thorium and uranium by miniaturized extraction chromatography: application to isotopic analyses of silicate rocks. *Anal. Chim. Acta* **339**, 79–89 (1997).
70. Chavagnac, V. et al. Towards the development of a fossil bone geochemical standard: an inter-laboratory study. *Anal. Chim. Acta* **599**, 177–190 (2007).
71. Scher, H. D. & Delaney, M. L. Breaking the glass ceiling for high resolution Nd isotope records in early Cenozoic paleoceanography. *Chem. Geol.* **269**, 329–338 (2010).
72. Thomas, D. J., Bralower, T. J. & Jones, C. E. Neodymium isotopic reconstruction of late Paleocene–early Eocene thermohaline circulation. *Earth Planet. Sci. Lett.* **209**, 309–322 (2003).
73. Martin, E. E. & Scher, H. A Nd isotopic study of southern sourced waters and Indonesian throughflow at intermediate depths in the Cenozoic Indian Ocean. *Geochem. Geophys. Geosystems* **7**, Q09N02 (2006).
74. Moiroud, M. et al. Evolution of the neodymium isotopic signature of neritic seawater on a northwestern Pacific margin: new constrains on possible end-members for the composition of deep-water masses in the Late Cretaceous ocean. *Chem. Geol.* **356**, 160–170 (2013).
75. Baatsen, M. et al. A generalised approach to reconstructing geographical boundary conditions for palaeoclimate modelling. *Clim. Past.* **12**, 4917–4942 (2016).